Ultra-High Field Birdcage Coils: a Comparison Study at 14.1T

Tian Cheng, Arthur W. Magill, Arnaud Comment, Rolf Gruetter and Hongxia Lei

Abstract— **An essential feature of magnetic resonance (MR) probes for magnetic resonance imaging and spectroscopy is the ability to generate uniform B_1^+ excitation in a volume of interest. When the magnetic field strength is increased, leading to an increase in resonance frequency, the constraints on the MR probes size, the sample size and the associated radiation losses caused by conductor elements are higher. In this study we simulate, test and construct two birdcage coils for imaging rodents operated at 14.1 T. Bench experiments and imaging tests show that at 14.1 T dielectric resonance effect is the dominant factor accounting for B_1^+ field inhomogeneity but remained achievable for imaging rodent brains.**

I. Introduction

Magnetic Resonance Imaging (MRI) is one of the most powerful non-invasive biomedical imaging methods which play an increasingly important role in clinical and research environments. To deliver morphological images with superb Signal-to-Noise (SNR) ratio, a good radio-frequency (RF) probe with a desired homogenous coverage is an essential compartment. As one of the classical designs of the RF probes, birdcage coil was first developed to deliver homogeneous whole body human images at relatively low magnetic field (1.5T) for clinical diagnostics several decades ago [1].

With the recent advent of ultra-high field (UHF) superconductive magnets and amplified interests in both human and animal models, the design of birdcage coils has become more technically challenging since the proton resonance frequency increases and the wavelength of the proton signal becomes shorter in air, and even shorter in biological tissue due to the high dielectric constant. When the sample size is comparable to this shortened wavelength, the dielectric resonance effect appears, which leads to a bright spot in the image [2-4]. Meanwhile RF radiation losses cannot be neglected due to a comparable conductor length to a fraction of the corresponding wavelength (normally $\lambda/20$) [5]. Indeed the birdcage coil has been limitedly used in the UHF for the human applications. Nevertheless for the pre-clinical research small animal, birdcage coils with a classical design can deliver sufficient RF homogeneity at 900MHz [6]. Besides the development of the multiple resonant birdcage coil also extends the applicability of the birdcage coil[7-9].

Two common architectures of the birdcage coil, namely high-pass (HP) and low-pass (LP) have been widely used for applications at numerous field strengths [10-12]. Besides the HP and LP, band-pass (BP, also called hybrid) coil, a mixture of HP and LP types, has segmentations on all coil elements [13, 14] and therefore can effectively reduce the RF losses at very high frequency. Till now such advantage of the BP in UHF applications has never been compared to either the HP or the LP. In this study we aimed to compare two different birdcage coils (HP and BP) with same dimensions for small animal MRI at 14.1T.

II. Methods

A. RF design and simulations of birdcage coils for rodent brains

Two birdcage resonators, one HP and one BP, were designed with 16 rungs (Outer diameter OD=50 mm, length L=32 mm, width of the rung W_{rung}=2 mm, width of the end ring W_{ring}=3 mm) and a RF shield (OD=94 mm, L=70 mm). RF models including each birdcage resonator with dimensions mentioned above and a phantom (L=80mm, elec. cond. 0.5 S/m) were built [7] (see Figure 1). After roughly calculating the tuning capacitor with Birdcage Builder [15], the RF model was simulated in 3D Electromagnetic simulation software (CST Microwave Studio, Darmstadt, Germany) to precisely approach the desired mode (m = 1) at 600MHz. Hexahedral mesh with 60 lines per wavelength was set to simulate the electrical and magnetic field distribution of the RF model with an accuracy of -40 dB in the transient solver. After fine tuning and matching both channels were decoupled at the desired frequencies by altering the balancing capacitor values. All calculated capacitor values were kept and used for building the coil prototype.

Due to the presence of the capacitors on the rungs in the BP model, an additional gap (W=2 mm) was added in the middle of the rungs. It has been reported previously that the BP mode distribution is dependent on the ratio between capacitance on the rung and capacitance on the end ring, C_{rung}/C_{ring} : when $C_{rung}/C_{ring} \gg 1$ the BP coil behaves as a HP

This work was supported by National Competence Center for Biomedical Imaging (NCCBI), Centre d'Imagerie Biomedicale (CIBM) of the UNIL, HUG, CHUV, EPFL and the Leenaards and Jeantet Foundations.

Tian Cheng is with dynamic nuclear polarization group (GR-CO) of the Institute of Physics of Biological Systems, École Polytechnique Fédérale de Lausanne, Lausanne, CH-1015, Switzerland (E-mail: tian.cheng@epfl.ch)

Arthur W. Magill is with CIBM-AIT, École Polytechnique Fédérale de Lausanne, Lausanne, CH-1015, Switzerland, on leave from the Forschungszentrum Jülich (E-mail: a.magill@fz-juelich.de)

Arnaud Comment is with dynamic nuclear polarization group (GR-CO) of the Institute of Physics of Biological Systems, École Polytechnique Fédérale de Lausanne, Lausanne, CH-1015, Switzerland (E-mail: arnaud.comment@epfl.ch)

Rolf Gruetter is with Laboratory of Functional and Metabolic Imaging, École Polytechnique Fédérale de Lausanne, Lausanne, CH-1015, Switzerland; Department of Radiology, University of Lausanne, Lausanne, CH-1015, Switzerland (E-mail: rolf.gruetter@epfl.ch)

Hongxia Lei is with CIBM-AIT, École Polytechnique Fédérale de Lausanne, Lausanne, CH-1015, Switzerland; Department of Radiology, University of Geneva, Geneva 14, CH-1211, Switzerland (Phone: +41 21 6937964, E-mail: hongxia.lei@epfl.ch)

978-1-4244-7929-0/14/$26.00 ©2014 IEEE

coil; when C_{rung} /C_{ring} «1 the BP coil tends to be a LP coil[13]. In practice *Crung* =2 pF was chosen for building the BP coil so that the capacitor value on the end rings could be within the range of available capacitance values.

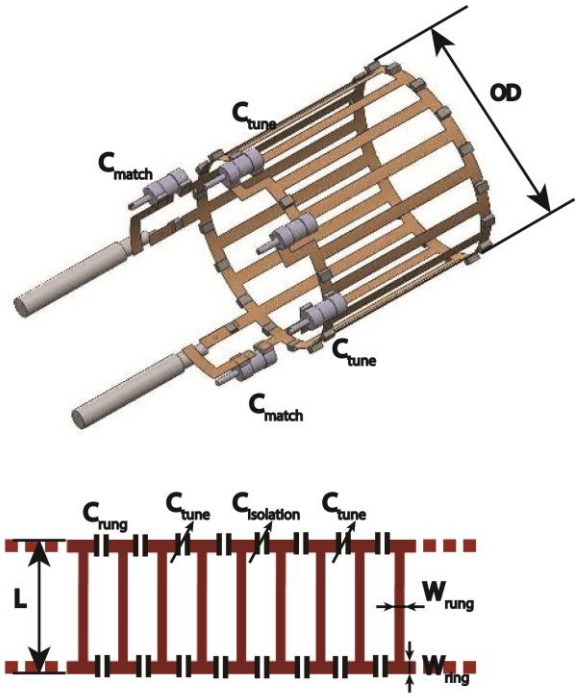

Figure 1. High-pass resonator with tuning and matching network.

B. RF coil components

The conducting structures of the coil prototypes were manufactured from flexible printed circuit board (0.1 mm FR4, 35 μm Cu) and then fixed on the inner support tube with an outer diameter of 50 mm (Acrylic glass (PMMA), Angst-Pfister, Switzerland). Ceramic chip capacitors (ATC-100B, American Technical Ceramics, USA) with the values properly simulated and five variable capacitors (NMKJ10HV, Voltronics, New York, USA) were used to tune birdcage coils to proper frequencies. 50-coaxial cables (Huber-Suhner, Switzerland) with pre-tuned bazooka baluns[16] were attached to the matching network of the coil to transmit/receive RF signals. RF shield of the coil was constructed by printing coaxial copper strips with small gap on both sides to reduce the eddy current and then taped inside the outer support tube with an inner diameter of 94 mm (PMMA, Angst-Pfister, Switzerland). The two support tubes were coaxially fixed by two plastic cover plates and non-magnetic screws.

C. Bench tests of the RF coils

To test the bench performance of these coils, a cylindrical phantom (OD=27 mm, L=100 mm) containing physiological saline solution (Sigma-Aldrich, USA) was fixed in the center of the coils. A plastic tube (L=250 mm, OD=120 mm) covered by copper sheet was used to cover the birdcage coil and simulate the magnet bore. Q-values were measured with a network analyzer (E5071C, Agilent, USA), with and without loading the phantom, by dividing the central frequency by the bandwidth measured at -7 dB [17] after tuning and matching two coils in which way full quality factor can be measured. Note that all the Q-values shown in this study were measured on-resonance with a -30 dB matching level.

D. Imaging and B_1^+ field mapping

All MR images were acquired in a horizontal 14.1 T magnet (31-cm-diameter, Agilent, USA). RF power calibrations were carried out using a STEAM sequence[18] with 0.5 ms asymmetric pulses. The maximum water peak intensity implied 90° power, $P_{90°}$. SNRs of the phantom images were determined by comparing the average intensity of multi-slice gradient echo (GRE) images with 90° flip angle in 5 different regions within a circle of 5 mm diameter with the noise acquired in the same areas after switching off the RF power amplifier. *In vivo* SNR maps at both field strengths were generated by using 60° GRE images through comparing the signal of each pixel to the standard deviation of noise in the artifact free corner region. Both SNR maps were rescaled by the maximum SNR value calculated. To maintain the thermal noise for both field strengths at the same level, spectral bandwidth of 69 kHz was set for both images.

To generate B_1^+ field maps, the double angle method [19, 20] was used. As the MR signal generated after a RF pulse with a flip angle α is proportional to sin α, the flip angle (FA) α can be calculated through comparing the signals acquired using two different FAs, α and 2 α, and is given by,

$$\alpha = \arccos(I_2/2I_1). \quad (1)$$

where I_1 and I_2 represent the signal intensity from coronal GRE images with flip angles of 60° and 120°, respectively (imaging parameters shown in Table I). A long enough repetition time of 20s was set to recover the proton magnetization. The region of interest in both phantom and *in vivo* brain measurements were shimmed using the fastestmap method [21]. Both images were post-processed using a MATLAB script which calculated the image intensity ratio from both acquisitions performed with different FAs and further determined the ratio pixel by pixel. An image mask was created by zero filling all the pixels with intensity less than 10% of the maximal pixel intensity and used to filter out noise on the B_1^+ distribution map.

TABLE I. GRE PARAMETERS USED FOR B_1^+ MAPPING

	TR/TE [ms]	***FOV [mm²]***	***Resolution***
Phantom	20,000/2.83	40*40	128*128
in vivo	20,000/3.31	20*20	128*128

III. Results and Discussion

A. Simulations of RF model

For both coils the capacitor values used in practice (C_{ring} = 8.2 pF and 12.6 pF HP and BP respectively) fit to the simulated capacitor values (C_{ring} = 8.5 pF and 12.5 pF for HP and BP respectively) very well. The small error comes from the stray capacitance caused by the matching network which was simulated separately in the CST Design Studio and not accounted for in the CST Microwave Studio simulation. This also explains the different matching capacitor values used in practice. In Figure 2, RF simulation of the B_1^+ field in cylindrical phantom positioned in the center of both coils are shown. It is apparent that the BP coil generates more homogeneous B_1^+ field.

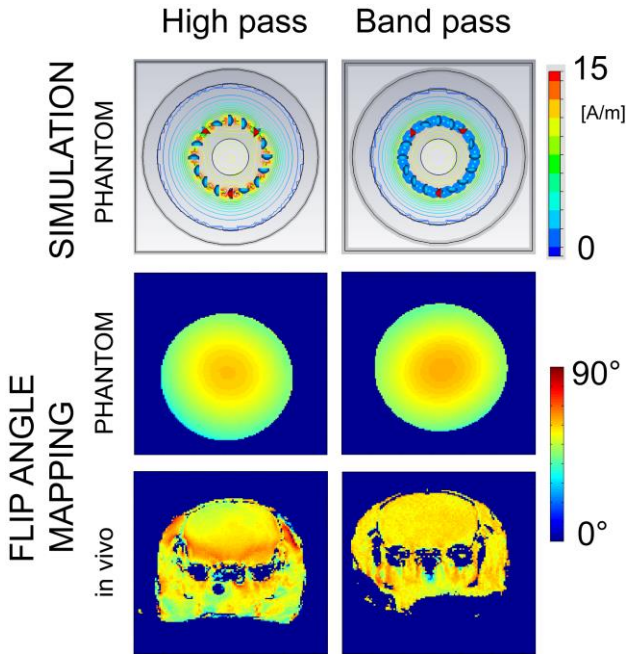

Figure 2. RF coil performance comparison (Results acquired with HP coil is shown in first row and with BP coil in second row): a) RF simulation (scaled from 0 to 15 A/m); b) B_1^+ mapping with a saline phantom using double angle method; c) *in vivo* B_1^+ mapping of mouse brains. Imaging parameters are given in table I. Due to the dielectric resonance of the phantom, only the central part can be taken as homogeneous. A slightly more homogeneous B_1^+ field was measured using BP coil.

B. Workbench measurements

Table II shows the measured Q-values of the built coils and their relative sensitivities. Since the coils were driven in a quadrature mode, good isolation between both channels is indeed necessary for reducing electric losses. The best isolation levels acquired by bench measurement were measured at -18 dB for loaded HP coils and at -30 dB for loaded BP coil. This means that only 1.6% of the RF power was dissipated not for RF excitation. Even when all the coils work in transceiver mode, the electric loss from the coils can be neglected. The low relative sensitivity in small animals is related to the small size of the brain causing a relatively low loading factor. Assuming the mouse brain has a cylindrical form with a diameter of 15mm, the filling factor is only around 9%.

TABLE II. Summary of coil bench measurements and calibration in phantom (Q_{UL} and Q_L stand for unloaded and loaded quality factors. $P_{90°}$ represents the power need for generate 90° Gaussian pulse with 2ms pulse length).

	Q_{UL}	Q_L	Rel. Sen.	$P_{90°}$ [dB]	FA [°]	SNR
HP	200	176	0.35	42	51±6	2207±252
BP	364	242	0.58	44	55±5	2369±232

C. B_1^+ field mapping

The RF power calibration was normalized to 2ms 90° Gaussian pulse and the measured FAs and SNRs are comparable as listed in table II. B_1^+ field mapping of both coils in coronal planes was performed with a saline phantom (27 mm OD) and *in vivo* in mouse brains at 14.1 T. Similar to the simulated results, the B_1^+ field measured in the phantom has a hot spot and only the coil center had the correct FA (Figure 2). Unlike the HP coil with such homogenous B_1^+ field covering a 11 mm OD area (~ 40% of 27 mm OD) , the BP coil presented the slightly larger homogenous B_1^+ field, i.e. 16 mm OD (~ 60% of 27 mm OD), as shown in Figure 2. This dimension is sufficient to cover the entire rat brain (i.e. 15*10*20 mm^3) and was confirmed by *in vivo* mouse brain results (Figure 2). Taking the relative electric permittivity ε=80 and conductivity σ= 0.5 S/m from the biological tissue into account, the wavelength in the tissue is reduced to 56 mm at 14.1 T. Thus, the hot spot was mainly due to the dielectric resonance effect.

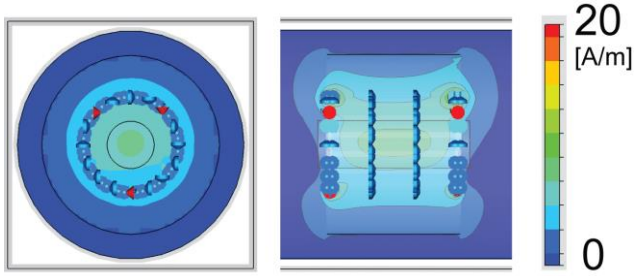

Figure 3. *RF simulation of a BP type birdcage coil in coronal (left) and sagittal (right) direction at 14.1 T with longer rung (L=70 mm):* B_1^+ *mapping showed a more homogeneous* B_1^+ *field for BP coil along coronal direction.*

In our study, the BP coil didn't show great difference in the total length of the coil comparing to the HP coil. Indeed, we aimed to reduce the required RF power and radiation effect of the conductors, the length of the coil was designed enough for imaging small rodent brains, i.e. 20-25 mm in rats and 10-12 mm in mice. Thus, both coils built in this study have the same length 30 mm so that the difference of the B_1^+ field in coronal direction was not striking between HP and BP coils (Figure 2).

The advantage of the BP coil can be first unveiled when the coil length is longer than the coil diameter or even wavelength. Simulation results showed that the B_1^+ field

distribution of long BP coil can be homogenous in the entire coil (Figure 3).

IV. Conclusion

In this study we demonstrate that it is possible to build transceiver bird cage coils suitable for imaging rodent brain at 14.1 T. The RF simulation was shown as a powerful tool for searching the right birdcage mode and can be trusted for further developments of the birdcage coils. The B_1^+ field homogeneity of the BP coil is better than the HP one used at 14.1 T due to less dielectric resonance effect and image SNR in the BP coil become also slightly better than that in the HP type. With the increase of the physical size of the coil and the working frequency, BP birdcage coil could be an alternative for ultra-high magnetic field small animal imaging.

References

[1] C. E. Hayes, W. A. Edelstein, J. F. Schenck, O. M. Mueller, and M. Eash, "An Efficient, Highly Homogeneous Radiofrequency Coil for Whole-Body Nmr Imaging at 1.5-T," *Journal of Magnetic Resonance,* vol. 63, pp. 622-628, 1985.

[2] J. Tropp, "Image brightening in samples of high dielectric constant," *Journal of Magnetic Resonance,* vol. 167, pp. 12-24, Mar 2004.

[3] P. Roschmann, "Radiofrequency Penetration and Absorption in the Human-Body - Limitations to High-Field Whole-Body Nuclear-Magnetic-Resonance Imaging," *Medical Physics,* vol. 14, pp. 922-931, Nov-Dec 1987.

[4] J. W. Carlson, "Radiofrequency Field Propagation in Conductive Nmr Samples," *Journal of Magnetic Resonance,* vol. 78, pp. 563-573, Jul 1988.

[5] C. N. Chen and D. I. Hoult, *Biomedical magnetic resonance technology*: Hilger, 1989.

[6] C. Qian, I. S. Masad, J. T. Rosenberg, M. Elumalai, W. W. Brey, S. C. Grant, and P. L. Gor'kov, "A volume birdcage coil with an adjustable sliding tuner ring for neuroimaging in high field vertical magnets: ex and in vivo applications at 21.1T," *J Magn Reson,* vol. 221, pp. 110-6, Aug 2012.

[7] J. Murphy-Boesch, "Double-Tuned Birdcage Coils: Construction and Tuning," in *Encyclopedia of Magnetic Resonance*, ed: John Wiley & Sons, Ltd, 2007.

[8] A. R. Rath, "Design and performance of a double-tuned bird-cage coil," *Journal of Magnetic Resonance (1969),* vol. 86, pp. 488-495, 2/15/ 1990.

[9] C. Wang, Y. Li, B. Wu, D. Xu, S. J. Nelson, D. B. Vigneron, and X. Zhang, "A practical multinuclear transceiver volume coil for in vivo MRI/MRS at 7 T," *Magn Reson Imaging,* vol. 30, pp. 78-84, Jan 2012.

[10] J. Tropp, "The Theory of the Bird-Cage Resonator," *Journal of Magnetic Resonance,* vol. 82, pp. 51-62, Mar 1989.

[11] R. J. Pascone, B. J. Garcia, T. M. Fitzgerald, T. Vullo, R. Zipagan, and P. T. Cahill, "Generalized electrical analysis of low-pass and high-pass birdcage resonators," *Magn Reson Imaging,* vol. 9, pp. 395-408, 1991.

[12] T. S. Ibrahim, R. Lee, B. A. Baertlein, and P. M. L. Robitaille, "B-1 field homogeneity and SAR calculations for the birdcage coil," *Physics in Medicine and Biology,* vol. 46, pp. 609-619, Feb 2001.

[13] J. Tropp, "The hybrid bird cage resonator," *Proceedings of the International Society for Magnetic Resonance in Medicine,* vol. 1992, p. 4009, 1992.

[14] P. Pimmel and A. Briguet, "A Hybrid Bird Cage Resonator for Sodium Observation at 4.7-T," *Magnetic Resonance in Medicine,* vol. 24, pp. 158-162, Mar 1992.

[15] C.-L. Chin, C. M. Collins, S. Li, B. J. Dardzinski, and M. B. Smith, "BirdcageBuilder: Design of specified-geometry birdcage coils with desired current pattern and resonant frequency," *Concepts in Magnetic Resonance,* vol. 15, pp. 156-163, 2002.

[16] J. Mispelter, M. Lupu, and A. Briguet, *NMR probeheads for biophysical and biomedical experiments : theoretical principles & practical guidelines*. London: Imperial College Press, 2006.

[17] A. Haase, F. Odoj, M. Von Kienlin, J. Warnking, F. Fidler, A. Weisser, M. Nittka, E. Rommel, T. Lanz, B. Kalusche, and M. Griswold, "NMR probeheads for in vivo applications," *Concepts in Magnetic Resonance,* vol. 12, pp. 361-388, 2000.

[18] J. Frahm, K. D. Merboldt, and W. Hanicke, "Localized Proton Spectroscopy Using Stimulated Echoes," *Journal of Magnetic Resonance,* vol. 72, pp. 502-508, May 1987.

[19] R. Stollberger, P. Wach, G. McKinnon, E. Justich, and F. Ebner, "RF-field mapping in vivo," in *Proceedings of the International Society for Magnetic Resonance in Medicine*, San Francisco, 1988, p. 106.

[20] E. K. Insko and L. Bolinger, "B1 mapping," in *Proceedings of the International Society for Magnetic Resonance in Medicine*, 1992, p. 4302.

[21] R. Gruetter, "Automatic, localized in vivo adjustment of all first- and second-order shim coils," *Magnetic Resonance in Medicine,* vol. 29, pp. 804-11, Jun 1993.